ACS APPLIED MATERIALS & INTERFACES

www.acsami.org

Research Article

$Ba_{1/3}CoO_2$: A Thermoelectric Oxide Showing a Reliable *ZT* of ~0.55 at 600 °C in Air

Xi Zhang,[‖] Yuqiao Zhang,*[,‖] Liao Wu, Akihiro Tsuruta, Masashi Mikami, Hai Jun Cho, and Hiromichi Ohta*

Cite This: *ACS Appl. Mater. Interfaces* 2022, 14, 33355–33360

Read Online

ACCESS | Metrics & More | Article Recommendations | Supporting Information

ABSTRACT: Thermoelectric energy conversion technology has attracted attention as an energy harvesting technology that converts waste heat into electricity by means of the Seebeck effect. Oxide-based thermoelectric materials that show a high figure of merit are promising because of their good chemical and thermal stability as well as their harmless nature compared to chalcogenide-based state-of-the-art thermoelectric materials. Although several high-*ZT* thermoelectric oxides (*ZT* > 1) have been reported thus far, the reliability is low due to a lack of careful observation of their stability at elevated temperatures. Here, we show a reliable high-*ZT* thermoelectric oxide, $Ba_{1/3}CoO_2$. We fabricated $Ba_{1/3}CoO_2$ epitaxial films by the reactive solid-phase epitaxy method ($Na_{3/4}CoO_2$) followed by ion exchange ($Na^+ \rightarrow Ba^{2+}$) treatment and performed thermal annealing of the film at high temperatures and structural and electrical measurements. The crystal structure and electrical resistivity of the $Ba_{1/3}CoO_2$ epitaxial films were found to be maintained up to 600 °C. The power factor gradually increased to ~1.2 mW m^{-1} K^{-2} and the thermal conductivity gradually decreased to ~1.9 W m^{-1} K^{-1} with increasing temperature up to 600 °C. Consequently, the *ZT* reached ~0.55 at 600 °C in air.

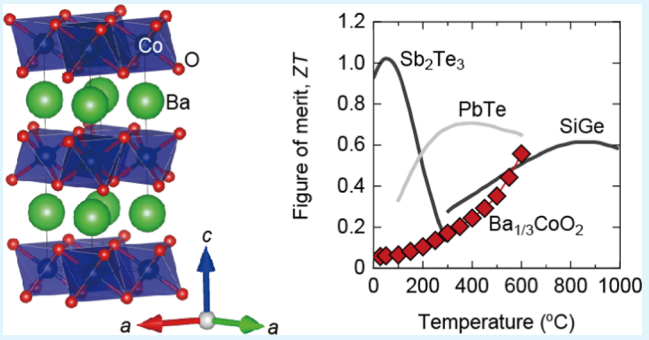

KEYWORDS: *$Ba_{1/3}CoO_2$, layered oxide, cobaltate, thermoelectric materials, figure of merit, thermal stability*

INTRODUCTION

Thermoelectric energy conversion technology has attracted attention as an energy harvesting technology that converts waste heat into electricity by means of the Seebeck effect.[1−3] The efficiency of the conversion from the temperature difference to electricity strongly depends on the thermoelectric figure of merit *ZT* ($=S^2 \cdot \sigma \cdot T \cdot \kappa^{-1}$, where *S* is the thermopower or Seebeck coefficient, σ is the electrical conductivity, *T* is the absolute temperature, and κ is the total thermal conductivity) of the thermoelectric materials. At present, practically available thermoelectric materials are n-type Bi_2Te_3 (*ZT* ~ 1 at 100 °C), n-type PbTe (*ZT* ~ 0.8 at 350 °C), n-type $CoSb_3$ (*ZT* ~ 0.8 at 550 °C), n-type SiGe (*ZT* ~ 1 at 900 °C), p-type Sb_2Te_3 (*ZT* ~ 1 at 50 °C), p-type PbTe (*ZT* ~ 0.7 at 400 °C), and p-type SiGe (*ZT* ~ 0.6 at 800 °C).[1] Since these *ZT* values are ~1, *ZT* = 1 is often called the threshold for practical application.

Since 2000, many efforts have been made to develop thermoelectric materials with high *ZT* (>1) such as lead chalcogenides,[4−6] skutterudites,[7−9] half-Heuslers,[10−12] and SnSe.[13−16] For example, an extremely high *ZT* of ~2.5 at 650 °C was obtained in the PbTe-SrTe system by non-equilibrium processing.[14] More recently, an even higher *ZT* value of 3.1 at 510 °C was achieved in hole-doped SnSe polycrystalline samples by carefully removing performance-unfavorable tin oxides.[16] Despite the progress made in thermoelectric materials, the practical applications of these materials are still limited due to the high cost of the rare elements involved and the shortage of natural resources (Te is one of the rarest elements on earth). In addition, most sulfides, selenides, and tellurides are toxic and thermally and chemically unstable. Developing good thermoelectric materials with high *ZT* without the above issues is essential for widespread use.

Since most metal oxides show good chemical and thermal stability in air as well as a harmless nature compared to chalcogenide-based state-of-the-art thermoelectric materials, oxide-based thermoelectric materials that show a high *ZT* are promising.[17,18] Several high-*ZT* thermoelectric oxides have been reported thus far; Fujita et al.[19] reported that the Na_xCoO_2 single crystal exhibited a *ZT* of ~1.2 at 800 K. Acharya et al.[20] reported that Nb-doped $SrTiO_3$ with natural graphite exhibited a *ZT* of ~1.42 at 1050 K. Biswas et al.[21] reported that graphene oxide-encapsulated ZnO nanocomposites exhibited a *ZT* of ~0.52 at 1100 K. However, the

Received: May 14, 2022
Accepted: June 28, 2022
Published: July 12, 2022

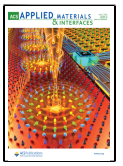

https://doi.org/10.1021/acsami.2c08555
ACS Appl. Mater. Interfaces 2022, 14, 33355−33360

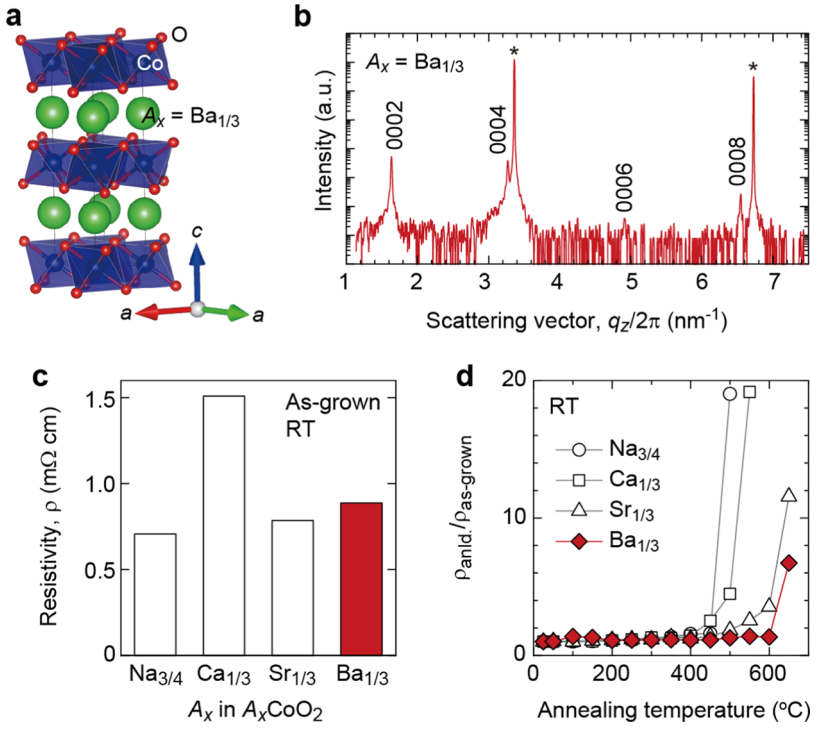

Figure 1. Change in the electrical resistivity (ρ) of A_xCoO_2 (A_x = $Na_{3/4}$, $Ca_{1/3}$, $Sr_{1/3}$, and $Ba_{1/3}$) films after annealing at high temperatures for 0.5 h in air. (a) Schematic crystal structure of A_xCoO_2 (A_x = $Ba_{1/3}$). (b) Out-of-plane XRD pattern of the A_xCoO_2 (A_x = $Ba_{1/3}$) film (as-grown). For other compositions, see Figure S1a–c. (c) ρ of the as-grown A_xCoO_2 films measured at room temperature. (d) Resistivity ratio of the thermally annealed sample/as-grown sample ($\rho_{anld}/\rho_{as\text{-}grown}$) measured at room temperature after each annealing step. The $\rho_{anld}/\rho_{as\text{-}grown}$ of the $Na_{3/4}CoO_2$ and $Ca_{1/3}CoO_2$ films starts to increase at 350 °C, that of the $Sr_{1/3}CoO_2$ film starts to increase at 450 °C, and that of the $Ba_{1/3}CoO_2$ film starts to increase at 650 °C.

reliability is considerably low due to a lack of careful observation of their stability at elevated temperatures.

To prevent misunderstanding of the thermoelectric properties as well as the chemical and thermal stability of oxide-based thermoelectric materials at high temperatures, we have thus far investigated this subject using epitaxial thin films of oxide-based thermoelectric materials.[22] Since the surface area of thin films is larger than that of bulk, thin films exhibit high sensitivity to the atmosphere. For example, an Al-doped ZnO epitaxial film evaporates at high temperatures (>600 °C) in air, indicating that the reported ZT values of ZnO-related thermoelectric oxides at high temperatures might be mostly invalid. Thus, reliable oxide-based thermoelectric materials that show high ZT (>1) at high temperatures have not yet been discovered.

To discover oxide-based thermoelectric materials that show high ZT, we firstly focused layered cobalt oxide $Na_{3/4}CoO_2$ that was discovered by Terasaki et al.[23] $Na_{3/4}CoO_2$ shows rather high power factor ($S^2\sigma$) whereas high κ, therefore ZT is low. We studied the thermoelectric properties of layered cobalt oxides A_xCoO_2 (A_x = $Na_{3/4}$, Li, $Ca_{1/3}$, $Sr_{1/3}$, and $Ba_{1/3}$) epitaxial films step by step as follows. Firstly, we developed the epitaxial film growth method of $Na_{3/4}CoO_2$ namely reactive solid phase epitaxy in 2005.[24] After that, we found that the Na ions in the $Na_{3/4}CoO_2$ films can be exchanged for Li,[25] Sr,[26] and Ca.[27] Further, we found that the layer can be inclined by using M-plane sapphire as the substrate.[28] Recently, we began to measure the in-plane κ of the films by the time domain thermoreflectance (TDTR) method. We hypothesized that a layered cobalt oxide composed of heavy ions shows low κ due to vibrational damping caused by the heavy ions while maintaining a high $S^2\sigma$.[29] As a result, we recently found that a $Ba_{1/3}CoO_2$ film exhibits a relatively high ZT of ∼0.11 at room temperature,[30] which is the highest among the reported oxide thermoelectric materials except for oxychalcogenide (BiO)(CuSe).[31] In this study, we systematically investigated the thermal stability of A_xCoO_2 (A_x = $Na_{3/4}$, $Ca_{1/3}$, $Sr_{1/3}$, and $Ba_{1/3}$) films at high temperature in air and clarified that $Ba_{1/3}CoO_2$ is stable up to 600 °C. Then, we measured the thermoelectric properties of $Ba_{1/3}CoO_2$ films up to 600 °C. Here, we show that $Ba_{1/3}CoO_2$ exhibits a reliable high ZT of 0.55 at 600 °C in air. This high ZT of $Ba_{1/3}CoO_2$ is reproducible and reliable, the highest among oxides and comparable to that of p-type PbTe and p-type SiGe. These results reveal that $Ba_{1/3}CoO_2$ would be a good candidate for a high-temperature thermoelectric material.

EXPERIMENTAL SECTION

Fabrication of A_xCoO_2 (A_x = $Na_{3/4}$, $Ca_{1/3}$, $Sr_{1/3}$, and $Ba_{1/3}$) Films. A_xCoO_2 epitaxial films were fabricated on (111) YSZ or $(1\bar{1}00)$ α-Al_2O_3 substrates by reactive solid-phase epitaxy (R-SPE) of $Na_{3/4}CoO_2$ films followed by ion exchange treatment. First, CoO films were heteroepitaxially grown on the substrate at 700 °C in an oxygen atmosphere (10^{-3} Pa) by a pulsed laser deposition technique (KrF excimer laser, ∼2 J cm^{-2} pulse^{-1}, 10 Hz). Then, the CoO film was heated with $NaHCO_3$ powder at 750 °C in air. This results in the formation of a $Na_{3/4}CoO_2$ epitaxial film. Then, the Na^+ ions in the resultant films were exchanged with Ca^{2+}, Sr^{2+}, and Ba^{2+} ions by applying the appropriate ion-exchange treatment. Details of the fabrication procedure have been published elsewhere.[24,26,27,29,30]

Crystallographic Analyses. The crystalline phase, orientation, and thickness of the resultant films were analysed by X-ray diffraction (XRD) (Cu Kα_1, ATX-G, Rigaku). Out-of-plane Bragg diffraction

https://doi.org/10.1021/acsami.2c08555
ACS Appl. Mater. Interfaces 2022, 14, 33355−33360

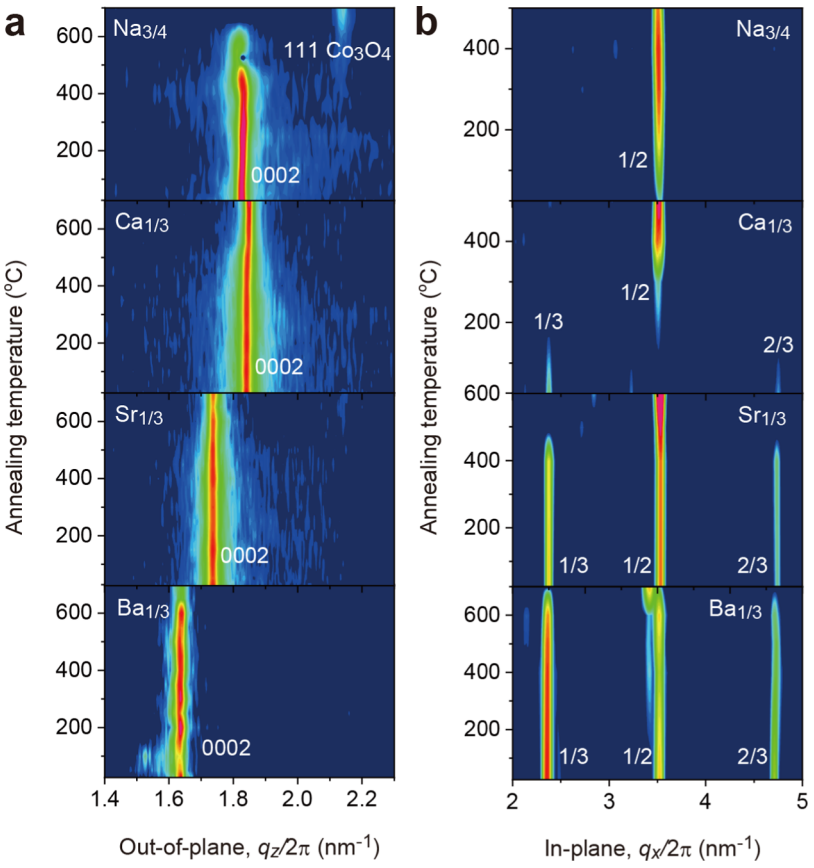

Figure 2. Change in the crystal structure of A_xCoO_2 (A_x = $Na_{3/4}$, $Ca_{1/3}$, $Sr_{1/3}$, and $Ba_{1/3}$) films after annealing at high temperatures for 0.5 h in air. (a) Out-of-plane XRD patterns measured at room temperature after each annealing step. The 0002 $Na_{3/4}CoO_2$ diffraction peak intensity decreases above 450 °C due to the decomposition into Co_3O_4 while remaining stable for $Ca_{1/3}CoO_2$, $Sr_{1/3}CoO_2$, and $Ba_{1/3}CoO_2$ up to 650 °C. (b) In-plane XRD patterns measured at room temperature after each annealing step. The 1/3 and 2/3 diffraction peaks of the $Ca_{1/3}CoO_2$ film disappear at approximately 200 °C, and the 1/2 diffraction peak appears above 200 °C. The 1/3 and 2/3 diffraction peaks of the $Sr_{1/3}CoO_2$ film disappear at approximately 450 °C, and the 1/2 diffraction peak appears above 450 °C. The 1/3 and 2/3 diffraction peaks of the $Ba_{1/3}CoO_2$ film are stable up to 600 °C.

patterns, in-plane Bragg diffraction patterns, rocking curves, and X-ray reflection patterns were acquired.

Resistivity and Thermopower Measurements. At room temperature and below room temperature, the electrical resistivity (ρ) or conductivity ($1/\rho$, σ) of films were measured by the dc four-probe method with the van der Pauw electrode configuration. The thermopower (S) was measured by the steady method. Homemade equipment was used for these measurements. Above room temperature, σ and S values were measured by thermoelectric measurement equipment (MODEL RZ2001i, Ozawa Science Co.).

Thermal Conductivity Measurement. The thermal conductivity (κ) of the films in the direction perpendicular to the substrate surface was measured by the time domain thermoreflectance (TDTR, PicoTR, PicoTherm Co.) method. Before the measurement, a dense Pt film was deposited on the surface of the A_xCoO_2 film as the transducer by dc sputtering at room temperature. The decay curves of TDTR signals were simulated to obtain the thermal conductivity. The specific heat capacity used for the TDTR simulation was measured using differential scanning calorimetry (DSC, DSC8500, PerkinElmer) (Supporting Information, Figure S3). The in-plane κ of the films was extracted according to the following equation as previously reported.[20,21]

$$\kappa_{obsd} = \sqrt{\kappa_{\parallel}^2 \cos^2 \varphi + \kappa_{\perp}^2 \sin^2 \varphi}$$

where φ, κ_{obsd}, $\kappa_{//}$ and $\kappa_{\perp}$ are the inclination angle of the layers relative to the perpendicular of the film surface, observed thermal conductivity, in-plane κ, and cross-plane κ, respectively (Supporting Information, Figure S4). In this study, φ = 35°, which was proven by scanning transmission electron microscopy (STEM) observations in our previous study.[21]

RESULTS AND DISCUSSION

Figure 1a schematically illustrates the crystal structure of A_xCoO_2 (A_x = $Ba_{1/3}$). The CoO_2 layer is composed of edge-sharing CoO_6 octahedra, and the A_x layer (A_x = $Na_{3/4}$, $Ca_{1/3}$, $Sr_{1/3}$, $Ba_{1/3}$) is alternately stacked along the c-axis. We fabricated 150-nm-thick c-axis oriented A_xCoO_2 (A_x = $Na_{3/4}$, $Ca_{1/3}$, $Sr_{1/3}$, and $Ba_{1/3}$) epitaxial films on (111) yttria stabilized zirconia (YSZ) substrates. Details of the fabrication procedure have been reported elsewhere.[24,26,27,29,30] Only an intense 0002 A_xCoO_2 diffraction peak is observed in the out-of-plane X-ray diffraction (XRD) patterns of the as-grown A_xCoO_2 films (Figures 1b and S1a–d). The c-axis lattice parameter was calculated to be as follows: $Na_{3/4}$ = 1.094 nm, $Ca_{1/3}$ = 1.087 nm, $Sr_{1/3}$ = 1.153 nm, and $Ba_{1/3}$ = 1.223 nm, which correspond well with a previous report.[30]

First, we clarified the stability of the resultant A_xCoO_2 (A_x = $Na_{3/4}$, $Ca_{1/3}$, $Sr_{1/3}$, and $Ba_{1/3}$) films at high temperatures in air. Before annealing, we measured the electrical resistivity (ρ) of the as-grown films at room temperature in air (Figure 1c). Note that the ρ of $Ca_{1/3}CoO_2$ was higher than that of $Sr_{1/3}CoO_2$ and $Ba_{1/3}CoO_2$. The carrier mobility of $Ca_{1/3}CoO_2$ decreases dramatically when the Ca arrangement is ortho-

https://doi.org/10.1021/acsami.2c08555
ACS Appl. Mater. Interfaces 2022, 14, 33355−33360

rhombic which occurs when the film is annealed above 300 °C.[27] Since the ion exchange treatment from Na to Ca is performed at 300 °C, there is a possibility that a tiny amount of orthorhombic arrangement of Ca formed during the ion exchange treatment. Then, we annealed the films at high temperatures and subsequently performed structural and electrical measurements at room temperature. Figure 1d shows the change in the ρ ratio of an annealed sample (ρ_{anld}) and the as-grown sample ($\rho_{as\text{-}grown}$) measured at room temperature after annealing at each temperature for 0.5 h in air. The $\rho_{anld}/\rho_{as\text{-}grown}$ of the $Na_{3/4}CoO_2$ and $Ca_{1/3}CoO_2$ films starts to increase at 350 °C, and the $\rho_{anld}/\rho_{as\text{-}grown}$ of the $Sr_{1/3}CoO_2$ film starts to increase at 450 °C, while that of the $Ba_{1/3}CoO_2$ film remains stable below 600 °C. Thus, the highest applicable temperatures in air for $Na_{3/4}CoO_2$, $Ca_{1/3}CoO_2$, $Sr_{1/3}CoO_2$, and $Ba_{1/3}CoO_2$ are 350, 350, 450, and 600 °C, respectively.

To clarify the origin of the resistivity increase, we performed crystallographic analyses of the annealed films. Figure 2a shows the changes in the out-of-plane XRD pattern of the A_xCoO_2 films measured at room temperature after annealing at each temperature for 0.5 h in air. The 0002 $Na_{3/4}CoO_2$ diffraction peak intensity decreases above 450 °C, and the 111 Co_3O_4 peak appears after that due to evaporation of high vapor pressure Na. In contrast, the 0002 $Ca_{1/3}CoO_2$, 0002 $Sr_{1/3}CoO_2$, and 0002 $Ba_{1/3}CoO_2$ peaks are clearly seen below 650 °C. Thus, the out-of-plane XRD patterns of $Ca_{1/3}CoO_2$, $Sr_{1/3}CoO_2$, and $Ba_{1/3}CoO_2$ are not sufficient to clarify the origin of the resistivity increase.

We then analysed the structural change in the A_xCoO_2 epitaxial films through in-plane XRD measurements. Figure S1e–h show the in-plane XRD patterns of the as-grown A_xCoO_2 epitaxial films. An intense $11\bar{2}0$ A_xCoO_2 diffraction peak is seen at $q_x/2\pi = 7.05$ nm^{-1} together with the $2\bar{2}0$ YSZ substrate peak in all cases, indicating that the lattice parameter a of the A_xCoO_2 epitaxial films is ∼0.284 nm. Several diffraction peaks with fractional diffraction indices are seen in the in-plane XRD patterns, indicating an ordered structure of the A ions. The fractional peak of $(11\bar{2}0) \times 1/2$ is from the orthorhombic lattice of the cation layer; the fractional peaks of $(11\bar{2}0) \times 1/3$ and 2/3 are from the hexagonal lattice.[32] Thus, in the as-grown state, the $Na_{3/4}CoO_2$ film belongs to the orthorhombic lattice, and the $Ca_{1/3}CoO_2$ film belongs to the hexagonal lattice; the $Sr_{1/3}CoO_2$ and $Ba_{1/3}CoO_2$ films belong to the hexagonal-orthorhombic hybridized lattice.

Figure 2b shows the in-plane XRD patterns of the A_xCoO_2 films measured at room temperature after annealing at each temperature for 0.5 h in air. The 1/3 and 2/3 diffraction peaks of the $Ca_{1/3}CoO_2$ film disappear at approximately 200 °C, and the 1/2 diffraction peak appears above 200 °C, revealing that a phase transition from hexagonal to orthorhombic occurs.[27] The $Sr_{1/3}CoO_2$ film shows a transition from the hexagonal-orthorhombic hybridized lattice to the orthorhombic lattice at ∼450 °C. The 1/3 and 2/3 diffraction peaks of the $Ba_{1/3}CoO_2$ film are stable up to 600 °C. From these results, we determined that the thermal stability of the ordered structure affects the electrical resistivity of A_xCoO_2 films.

Then, we measured the thermoelectric properties of the A_xCoO_2 (A_x = $Na_{3/4}$, $Ca_{1/3}$, $Sr_{1/3}$, and $Ba_{1/3}$) films (as-grown samples) in the in-plane direction at high temperatures in air. The room-temperature electrical conductivity (σ) of $Na_{3/4}$ is ∼1400 S cm^{-1}, $Ca_{1/3}$ is ∼670 S cm^{-1}, $Sr_{1/3}$ is ∼1250 S cm^{-1}, and $Ba_{1/3}$ is 1100 S cm^{-1} (Figure 3a), which are slightly smaller

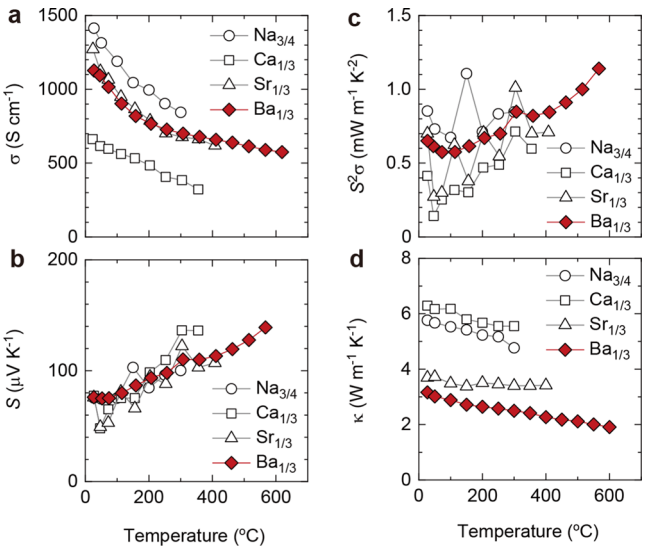

Figure 3. Thermoelectric properties of A_xCoO_2 (A_x = $Na_{3/4}$, $Ca_{1/3}$, $Sr_{1/3}$, and $Ba_{1/3}$) epitaxial films measured in the in-plane direction. (a) Electrical conductivity (σ). (b) Thermopower (S). (c) Power factor ($S^2\sigma$). (d) Thermal conductivity (κ). In all cases, σ decreases with temperature, while S increases with temperature. The $S^2\sigma$ values first decrease and then increase with temperature. κ slightly decreases with temperature in all cases. Note that in the case of the $Ba_{1/3}CoO_2$ film, $S^2\sigma$ is ∼1.2 mW m^{-1} K^{-2} and κ is ∼1.9 W m^{-1} K^{-1} at 600 °C in air.

than those of the films grown on (0001) α-Al_2O_3 substrates.[30] σ gradually decreases with temperature, showing the metallic nature of the films. In contrast, the thermopower (S) of the A_xCoO_2 films is ∼80 μV K^{-1} at room temperature in all cases and linearly increases with temperature (Figure 3b). This T-linear increase of S is due to the metallic nature of the films. The low-temperature thermoelectric properties (Figure S2) support this conclusion. Although there is a difference in σ between $Ca_{1/3}$ and the others, S does not reflect the difference in σ, indicating that the carrier relaxation time of $Ca_{1/3}$ is shorter than that of the others.

In this study, we used (111) YSZ as the substrate. The lateral grain size of the films on (111) YSZ is smaller than that of the films grown on (0001) α-Al_2O_3 substrates. In the case of (0001) α-Al_2O_3 substrates, an amorphous Na-Al-O layer is formed between the film and the substrate during $Na_{3/4}CoO_2$ film growth.[33] Therefore, the cobaltite films release epitaxial strain in the case of α-Al_2O_3 substrates, and lateral grain growth occurs. In contrast, such an amorphous layer is not formed in the case of the (111) YSZ substrate. Therefore, lateral grain growth is suppressed and the carrier mobility is suppressed due to the grain boundaries at lower temperatures.

Next, we calculated the thermoelectric power factor ($S^2\sigma$) using the observed σ and S (Figure 3c). The room-temperature $S^2\sigma$ of $Na_{3/4}$ is ∼0.87 mW m^{-1} K^{-2}, $Ca_{1/3}$ is ∼0.43 mW m^{-1} K^{-2}, $Sr_{1/3}$ is ∼0.72 mW m^{-1} K^{-2}, and $Ba_{1/3}$ is ∼0.70 mW m^{-1} K^{-2}, which are smaller than those in our previous report (∼1.2 mW m^{-1} K^{-2} in all cases[30]) due to the smaller σ and S. $S^2\sigma$ decreases and increases with temperature. Note that the $S^2\sigma$ of the $Ba_{1/3}CoO_2$ film reaches ∼1.2 mW m^{-1} K^{-2} at approximately 600 °C in air.

Then, we estimated the temperature dependence of the thermal conductivity (κ) of A_xCoO_2 films grown on (111) YSZ and $(1\bar{1}00)$ α-Al_2O_3 substrates in the in-plane direction (Figure 3d). The room-temperature κ of $Na_{3/4}$ is ∼5.7 W m^{-1}

https://doi.org/10.1021/acsami.2c08555
ACS Appl. Mater. Interfaces 2022, 14, 33355−33360

K^{-1}, $Ca_{1/3}$ is ~6.3 W m^{-1} K^{-1}, $Sr_{1/3}$ is ~3.7 W m^{-1} K^{-1}, and $Ba_{1/3}$ is ~3.2 W m^{-1} K^{-1}. Regardless of the composition of A_x, all κ values decreased gradually with increasing temperature, suggesting heat conduction dominated by phonon-phonon scattering mechanism commonly observed at elevated temperatures. The κ of the $Ba_{1/3}CoO_2$ film reaches ~1.9 W m^{-1} K^{-1} at 600 °C in air.

Finally, we calculated the figure of merit ZT of the A_xCoO_2 films (Figure 4a). The room-temperature ZT value of A_xCoO_2

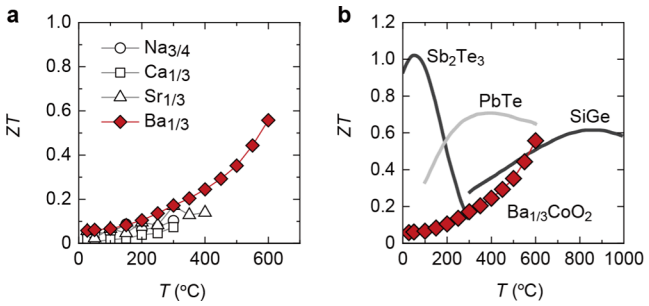

Figure 4. Temperature dependence of the ZT of the $Ba_{1/3}CoO_2$ epitaxial film in the in-plane direction. (a) Comparison among the four A_xCoO_2 (A_x = $Na_{3/4}$, $Ca_{1/3}$, $Sr_{1/3}$, and $Ba_{1/3}$) films. ZT increases with increasing temperature in all cases. The $Ba_{1/3}CoO_2$ epitaxial film has the highest ZT among the four A_xCoO_2 epitaxial films and reaches a high ZT value of ~0.55 at 600 °C. (b) Comparison against commercially available p-type thermoelectric materials (ref 1). The ZT of the $Ba_{1/3}CoO_2$ epitaxial film at 600 °C is comparable to that of p-type PbTe and p-type SiGe.

films is less than 0.06, but it dramatically increases with temperature. The ZT of $Ba_{1/3}CoO_2$ reaches 0.55 at approximately 600 °C in air. This high ZT of $Ba_{1/3}CoO_2$ is reproducible and reliable, the highest among oxides and comparable to that of p-type PbTe and p-type SiGe (Figure 4b). These results reveal that $Ba_{1/3}CoO_2$ would be a good candidate for a high-temperature thermoelectric material.

CONCLUSIONS

In summary, we discovered a reliable high-ZT thermoelectric oxide, $Ba_{1/3}CoO_2$. We clarified the stability of the $Ba_{1/3}CoO_2$ films at high temperatures in air and found that the crystal structure and electrical resistivity of $Ba_{1/3}CoO_2$ were maintained up to 600 °C. The power factor of $Ba_{1/3}CoO_2$ gradually increased to ~1.2 mW m^{-1} K^{-2} and the thermal conductivity gradually decreased to ~1.9 W m^{-1} K^{-1} with increasing temperature up to 600 °C. Consequently, ZT reached ~0.55 at 600 °C in air. This high ZT of $Ba_{1/3}CoO_2$ is reproducible and reliable (see Figure S5), the highest among oxides and comparable to that of p-type PbTe and p-type SiGe. These results reveal that $Ba_{1/3}CoO_2$ would be a good candidate for a high-temperature thermoelectric material.

ASSOCIATED CONTENT

Supporting Information

The Supporting Information is available free of charge at https://pubs.acs.org/doi/10.1021/acsami.2c08555.

Additional experimental details including XRD patterns of A_xCoO_2 (A_x = $Na_{3/4}$, $Ca_{1/3}$, $Sr_{1/3}$, and $Ba_{1/3}$) epitaxial films grown on (111) YSZ substrates; low-temperature thermoelectric properties of A_xCoO_2 (A_x = $Na_{3/4}$, $Ca_{1/3}$, $Sr_{1/3}$, and $Ba_{1/3}$) epitaxial films grown on (111) YSZ substrates; temperature-dependent specific heat capacity (C_p) of A_xCoO_2 (A_x = $Na_{3/4}$, $Ca_{1/3}$, $Sr_{1/3}$, and $Ba_{1/3}$) powders; thermal conductivity (κ) of A_xCoO_2 (A_x = $Na_{3/4}$, $Ca_{1/3}$, $Sr_{1/3}$, and $Ba_{1/3}$) epitaxial films grown on (111) YSZ or (1$\bar{1}$00) α-Al_2O_3 substrates (PDF)

AUTHOR INFORMATION

Corresponding Authors

Yuqiao Zhang − *Research Institute for Electronic Science, Hokkaido University, Kita, Sapporo 001-0020, Japan;* orcid.org/0000-0001-7579-4923; Email: yuqiaozhang0730@hotmail.com

Hiromichi Ohta − *Research Institute for Electronic Science, Hokkaido University, Kita, Sapporo 001-0020, Japan;* orcid.org/0000-0001-7013-0343; Email: hiromichi.ohta@es.hokudai.ac.jp

Authors

Xi Zhang − *Research Institute for Electronic Science, Hokkaido University, Kita, Sapporo 001-0020, Japan*

Liao Wu − *Graduate School of Information Science and Technology, Hokkaido University, Kita, Sapporo 060-0814, Japan*

Akihiro Tsuruta − *Innovative Functional Materials Research Institute, National Institute of Advanced Industrial Science and Technology (AIST), Moriyama, Nagoya 463-8560, Japan;* orcid.org/0000-0003-0674-3377

Masashi Mikami − *Innovative Functional Materials Research Institute, National Institute of Advanced Industrial Science and Technology (AIST), Moriyama, Nagoya 463-8560, Japan*

Hai Jun Cho − *Research Institute for Electronic Science, Hokkaido University, Kita, Sapporo 001-0020, Japan;* orcid.org/0000-0002-8642-4183

Complete contact information is available at: https://pubs.acs.org/10.1021/acsami.2c08555

Author Contributions

‖X.Z. and Y.Z. contributed equally to this work, and both are cited as first authors.

Author Contributions

X.Z., Y.Z., and L.W. fabricated the samples and measured the thermoelectric properties. A.T. and M.M. measured the electrical conductivity and thermopower at high temperatures. H.J.C. analysed the TDTR data. H.O. planned and supervised the project. All authors discussed the results and commented on the manuscript.

Funding

Hiromichi Ohta received founding from Grants-in-Aid of the JSPS (19H05788 and 22H00253).

Notes

The authors declare no competing financial interest.

ACKNOWLEDGMENTS

This research was supported by Grants-in-Aid for Innovative Areas (19H05791) from the Japan Society for the Promotion of Science (JSPS). H.O. is supported by a Grant-in-Aid for Scientific Research A (22H00253) from JSPS.

REFERENCES

(1) Snyder, G. J.; Toberer, E. S. Complex thermoelectric materials. *Nat. Mater.* **2008**, *7*, 105−114.

(2) He, J.; Tritt, T. M. Advances in thermoelectric materials research: Looking back and moving forward. *Science* **2017**, *357*, No. eaak9997.
(3) Shi, X.-L.; Zou, J.; Chen, Z.-G. Advanced thermoelectric design: from materials and structures to devices. *Chem. Rev.* **2020**, *120*, 7399−7515.
(4) Heremans, J. P.; Jovovic, V.; Toberer, E. S.; Saramat, A.; Kurosaki, K.; Charoenphakdee, A.; Yamanaka, S.; Snyder, G. J. Enhancement of thermoelectric efficiency in PbTe by distortion of the electronic density of states. *Science* **2008**, *321*, 554−557.
(5) Pei, Y.; Shi, X.; LaLonde, A.; Wang, H.; Chen, L.; Snyder, G. J. Convergence of electronic bands for high performance bulk thermoelectrics. *Nature* **2011**, *473*, 66−69.
(6) Biswas, K.; He, J.; Blum, I. D.; Wu, C.-I.; Hogan, T. P.; Seidman, D. N.; Dravid, V. P.; Kanatzidis, M. G. High-performance bulk thermoelectrics with all-scale hierarchical architectures. *Nature* **2012**, *489*, 414−418.
(7) Shi, X.; Yang, J.; Salvador, J. R.; Chi, M.; Cho, J. Y.; Wang, H.; Bai, S.; Yang, J.; Zhang, W.; Chen, L. Multiple-filled skutterudites: high thermoelectric figure of merit through separately optimizing electrical and thermal transports. *J. Am. Chem. Soc.* **2011**, *133*, 7837−7846.
(8) Tang, Y.; Gibbs, Z. M.; Agapito, L. A.; Li, G.; Kim, H.-S.; Nardelli, M. B.; Curtarolo, S.; Snyder, G. J. Convergence of multi-valley bands as the electronic origin of high thermoelectric performance in $CoSb_3$ skutterudites. *Nat. Mater.* **2015**, *14*, 1223−1228.
(9) Zhao, W.; Liu, Z.; Sun, Z.; Zhang, Q.; Wei, P.; Mu, X.; Zhou, H.; Li, C.; Ma, S.; He, D.; et al. Superparamagnetic enhancement of thermoelectric performance. *Nature* **2017**, *549*, 247−251.
(10) Zhu, H.; He, R.; Mao, J.; Zhu, Q.; Li, C.; Sun, J.; Ren, W.; Wang, Y.; Liu, Z.; Tang, Z.; et al. Discovery of ZrCoBi based half Heuslers with high thermoelectric conversion efficiency. *Nat. Commun.* **2018**, *9*, No. 2497.
(11) Zhu, H.; Mao, J.; Li, Y.; Sun, J.; Wang, Y.; Zhu, Q.; Li, G.; Song, Q.; Zhou, J.; Fu, Y.; et al. Discovery of TaFeSb-based half-Heuslers with high thermoelectric performance. *Nat. Commun.* **2019**, *10*, No. 270.
(12) Hinterleitner, B.; Knapp, I.; Poneder, M.; Shi, Y.; Müller, H.; Eguchi, G.; Eisenmenger-Sittner, C.; Stöger-Pollach, M.; Kakefuda, Y.; Kawamoto, N.; et al. Thermoelectric performance of a metastable thin-film Heusler alloy. *Nature* **2019**, *576*, 85−90.
(13) Zhao, L.-D.; Tan, G.; Hao, S.; He, J.; Pei, Y.; Chi, H.; Wang, H.; Gong, S.; Xu, H.; Dravid, V. P.; et al. Ultrahigh power factor and thermoelectric performance in hole-doped single-crystal SnSe. *Science* **2016**, *351*, 141−144.
(14) Tan, G.; Shi, F.; Hao, S.; Zhao, L.-D.; Chi, H.; Zhang, X.; Uher, C.; Wolverton, C.; Dravid, V. P.; Kanatzidis, M. G. Non-equilibrium processing leads to record high thermoelectric figure of merit in PbTe−SrTe. *Nat. Commun.* **2016**, *7*, No. 12167.
(15) Chang, C.; Wu, M.; He, D.; Pei, Y.; Wu, C.-F.; Wu, X.; Yu, H.; Zhu, F.; Wang, K.; Chen, Y.; et al. 3D charge and 2D phonon transports leading to high out-of-plane *ZT* in n-type SnSe crystals. *Science* **2018**, *360*, 778−783.
(16) Zhou, C.; Lee, Y. K.; Yu, Y.; Byun, S.; Luo, Z.-Z.; Lee, H.; Ge, B.; Lee, Y.-L.; Chen, X.; Lee, J. Y.; et al. Polycrystalline SnSe with a thermoelectric figure of merit greater than the single crystal. *Nat. Mater.* **2021**, *20*, 1378−1384.
(17) Fergus, J. W. Oxide materials for high temperature thermoelectric energy conversion. *J. Eur. Ceram. Soc.* **2012**, *32*, 525−540.
(18) Koumoto, K.; Funahashi, R.; Guilmeau, E.; Miyazaki, Y.; Weidenkaff, A.; Wang, Y. F.; Wan, C. L. Thermoelectric Ceramics for Energy Harvesting. *J. Am. Ceram. Soc.* **2013**, *96*, 1−23.
(19) Fujita, K.; Mochida, T.; Nakamura, K. High-temperature thermoelectric properties of $Na_xCoO_{2-\delta}$ single crystals. *Jpn. J. Appl. Phys.* **2001**, *40*, 4644−4647.
(20) Acharya, M.; Jana, S. S.; Ranjan, M.; Maiti, T. High performance (ZT > 1) n-type oxide thermoelectric composites from earth abundant materials. *Nano Energy* **2021**, *84*, No. 105905.
(21) Biswas, S.; Singh, S.; Singh, S.; Chattopadhyay, S.; de Silva, K. K. H.; Yoshimura, M.; Mitra, J.; Kamble, V. B. Selective Enhancement in Phonon Scattering Leads to a High Thermoelectric Figure-of-Merit in Graphene Oxide-Encapsulated ZnO Nanocomposites. *ACS Appl. Mater. Interfaces* **2021**, *13*, 23771−23786.
(22) Ohta, H.; Sugiura, K.; Koumoto, K. Recent progress in oxide thermoelectric materials: p-type $Ca_3Co_4O_9$ and n-type $SrTiO_3$. *Inorg. Chem.* **2008**, *47*, 8429−8436.
(23) Terasaki, I.; Sasago, Y.; Uchinokura, K. Large thermoelectric power in $NaCo_2O_4$ single crystals. *Phys. Rev. B* **1997**, *56*, 12685−12687.
(24) Ohta, H.; Kim, S. W.; Ohta, S.; Koumoto, K.; Hirano, M.; Hosono, H. Reactive solid-phase epitaxial growth of Na_xCoO_2 ($x \sim 0.83$) via lateral diffusion of Na into a cobalt oxide epitaxial layer. *Cryst. Growth Des.* **2005**, *5*, 25−28.
(25) Mizutani, A.; Sugiura, K.; Ohta, H.; Koumoto, K. Epitaxial film growth of Li_xCoO_2 ($0.6 < x < 0.9$) via topotactic ion exchange of $Na_{0.8}CoO_2$. *Cryst. Growth Des.* **2008**, *8*, 755−758.
(26) Sugiura, K.; Ohta, H.; Nomura, K.; Hirano, M.; Hosono, H.; Koumoto, K. Fabrication and thermoelectric properties of layered cobaltite, γ-$Sr_{0.32}Na_{0.21}CoO_2$ epitaxial films. *Appl. Phys. Lett.* **2006**, *88*, No. 082109.
(27) Sugiura, K.; Ohta, H.; Ishida, Y.; Huang, R.; Saito, T.; Ikuhara, Y.; Nomura, K.; Hosono, H.; Koumoto, K. Structural Transformation of Ca-Arrangements and Carrier Transport Properties in $Ca_{0.33}CoO_2$ Epitaxial Films. *Appl. Phys. Express* **2009**, *2*, No. 035503.
(28) Sugiura, K.; Ohta, H.; Nakagawa, S.; Huang, R.; Ikuhara, Y.; Nomura, K.; Hosono, H.; Koumoto, K. Anisotropic carrier transport properties in layered cobaltate epitaxial films grown by reactive solid-phase epitaxy. *Appl. Phys. Lett.* **2009**, *94*, No. 152105.
(29) Cho, H. J.; Takashima, Y.; Nezu, Y.; Onozato, T.; Ohta, H. Anisotropic heat conduction in ion-substituted layered cobalt oxides. *Adv. Mater. Interfaces* **2020**, *7*, No. 1901816.
(30) Takashima, Y.; Zhang, Y.; Wei, J.; Feng, B.; Ikuhara, Y.; Cho, H. J.; Ohta, H. Layered cobalt oxide epitaxial films exhibiting thermoelectric *ZT* = 0.11 at room temperature. *J. Mater. Chem. A* **2021**, *9*, 274−280.
(31) Zhao, L. D.; He, J. Q.; Berardan, D.; Lin, Y. H.; Li, J. F.; Nan, C. W.; Dragoe, N. BiCuSeO oxyselenides: new promising thermoelectric materials. *Energy Environ. Sci.* **2014**, *7*, 2900−2924.
(32) Huang, R.; Mizoguchi, T.; Sugiura, K.; Nakagawa, S.; Ohta, H.; Saito, T.; Koumoto, K.; Hirayama, T.; Ikuhara, Y. Microstructure evolution of $Ca_{0.33}CoO_2$ thin films investigated by high-angle annular dark-field scanning transmission electron microscopy. *J. Mater. Res.* **2009**, *24*, 279−287.
(33) Ohta, H.; Mizutani, A.; Sugiura, K.; Hirano, M.; Hosono, H.; Koumoto, K. Surface modification of glass substrates for oxide heteroepitaxy: Pasteable three-dimensionally oriented layered oxide thin films. *Adv. Mater.* **2006**, *18*, No. 1649.

https://doi.org/10.1021/acsami.2c08555
ACS Appl. Mater. Interfaces 2022, 14, 33355−33360